# Soret and Dufour Effect on Double Diffusive Natural Convection in a Wavy Porous Enclosure

B. V. R. Kumar[1,2,3], S.Belouettar[2], S. K. Murthy[1], Vivek Sangwan[1], Mohit Nigam[1], Shalini[4], D.A.S.Rees[5] and P.Chandra[1]
Indian Institute of Technology Kanpur, UP-208016, India[1]
CRP Henri Tudor, LTI, 29 Ave. J.F.K, L-1855, Luxembourg[2]
ITWM, Fraunhofer Institute I, Kaiserslautern, Germany[3]
INRIA, Rocquencourt, BP 105, 78153, Le Chesnay, France[4]
University of Bath, Bath, BA2 7AY, UK[5]

## Abstract

In this study the influence of Soret and Dufour effects on the double diffusive natural convection induced by an heated isothermal wavy vertical surface in a fluid saturated porous enclosure under Darcian assumptions has been analysed. The mathematical model has been solved numerically by finite element method and the simulations are carried out for various values of parameters such as $D_f$ (Dufour Number), $S_r$ (Soret Number), *Le* (Lewis Number), *B* (Buoyancy Number) and *N* (Number of waves per unit length) at small values of *Ra* (Rayleigh Number).

# Nomenclature

| | |
|---|---|
| $a$ | amplitude of the wavy wall |
| $g$ | gravitational acceleration |
| $k$ | thermal conductivity |
| $K$ | permeability of the medium |
| $K_T$ | thermal diffusion ratio |
| $C_s$ | concentration susceptibility |
| $C_p$ | specific heat at constant pressure |
| $L$ | the length or the mean width of the porous cavity |
| $n$ | outward drawn unit normal to the wavy surface |
| $N$ | number of waves considered per unit length |
| $Nu$ | Nusselt number |
| Sh | Sherwood Number |
| Q | cumulative heat flux |
| $Ra$ | Rayleigh number, $(Kg\beta\Delta tL)/\nu\alpha$ based on the dimension of porous cavity |
| Le | Lewis Number |
| B | Buoyancy Ratio |
| D | Mass Diffusivity |
| $QH_X$ | Cumulative Heat flux |
| $QM_X$ | Cumulative Mass flux |
| $S(\xi)$ | arc length of the wavy wall |
| $t$ | temperature |
| $T$ | non-dimensional temperature |
| $u,v$ | velocity components in x and y directions |
| $U,V$ | non-dimensional velocity component in X and Y directions |
| $V_c$ | convective velocity, $(g\beta K\Delta t)/\nu$ |

$w$ weight function used in finite element formulation
$x,y$ cartesian co-ordinates
$X,Y$ non-dimensional cartesian co-ordinates

**Greek Symbols:**

$\alpha$ thermal diffusivity constant
$\beta$ thermal expansion constant
$\rho$ fluid density
$\psi$ non-dimensional stream function
$\nu$ fluid kinematic viscosity
$\xi$ arc length variable
$\Omega$ the domain considered in the problem
$\Gamma$ the boundary of the domain

**Subscripts:**

f for fluid
w evaluated at the wall temperature
a evaluated at the ambient medium

# 1. Introduction

Study of coupled heat and mass transfer by natural convection in a fluid saturated porous medium has attracted considerable attention in a wide range of fields like oceanography, astrophysics, geology, nuclear engineering, chemical processes etc. It has gained lot significance due to it direct relevance in applications such as contaminant transport in ground water, nuclear waste management, separation process in chemical engineering, reservoirs of crude oil, geo-thermal reservoirs etc. A number of investigations have been carried out on Double Diffusive (DD) free convection process in a fluid saturated porous medium under various assumptions [1-6].

Diffusion of matter caused by temperature gradients (Soret Effect) and diffusion of heat caused by concentration gradients (Dufour Effect) become significant when temperature and concentration gradients are very large. Generally these effects are considered as second order phenomenon. Eckert and Drake [7], Zimmerman and Muller [8], Hurle and Jackerman [9], Bergman and Srinivasan [10], Weaver and Viskanta [11], Benano-Melly et al [12] etc., have investigated the importance of these effects on the convective heat transfer in fluids. However, regarding their influence on the DD free convection in a porous media not much has been reported in the literature. Anghel et al [13], Postelnicu [14], Sovran et al [15], Partha et al [16] etc. have investigated analytically the influence of either one or both of these effects on free convection flow induced by an isothermal

vertical surface in an electrically conducting Darcian fluid saturated porous medium under boundary layer assumptions.

Attachment of baffles, fins or other suitable protrusion to the hot surface of fluid saturated porous enclosure can affect convection process in the system and the process is used in several engineering applications related to building technology, cold storage units etc. Semi-conductor devices are intentionally roughened to alter their heat transfer capabilities. Riley [17], Rees and Pop [18-19], Murthy et al [20], Rathish Kumar [21-22] etc., have attempted to analyze natural convection heat transfer in porous media approximating the surface undulations by periodic functions.

In this study we consider a fluid saturated wavy porous enclosure under Darcian assumptions without any boundary layer assumptions. The coupled nonlinear partial differential equations, modelling the influence of Soret and Dufour effect on DD natural convection process in the vertical wavy enclosure, are solved numerically by Galerkin finite element method. Simulations are carried out for various values of $D_f, S_r, Le, N$ and $B$ and the results are depicted through streamlines, isotherms, iso-concentration contours and *xy*-plots.

## 2. Mathematical Model

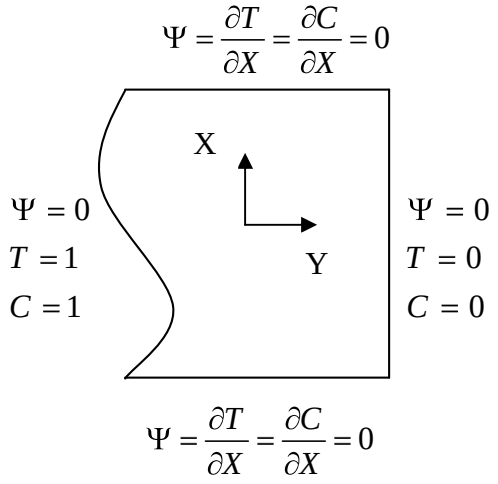



Fig. 1

Consider a fluid saturated isotropic homogenous porous enclosure (fig.1) with a wavy left vertical surface at a constant temperature $t_w$ and a constant wall concentration $c_w$. The right vertical wall is maintained at the ambient temperature $t_a$ ( $< t_w$ ) and at the ambient concentration $c_a$ ( $< c_w$ ). The fluid is assumed to satisfy the Boussinesq approximation and the flow is assumed to follow the Darcy law. Following Lai and Kulacki [10], Angirasa et al [11], Postelnicu [8], Partha [12] etc. the equations governing the heat and mass transfer process in the presence of Soret and Dufour effects, in non-dimensional form are written as follows:

$$\left(\frac{\partial^2\psi}{\partial x^2}+\frac{\partial^2\psi}{\partial y^2}\right)=\frac{\partial T}{\partial y}+B\frac{\partial C}{\partial y} \tag{1}$$

$$\frac{\partial\psi}{\partial y}\frac{\partial T}{\partial x}-\frac{\partial\psi}{\partial x}\frac{\partial T}{\partial y}=\frac{1}{Ra}\nabla^2 T+D_f\nabla^2 C \tag{2}$$

$$\frac{\partial\psi}{\partial y}\frac{\partial C}{\partial x}-\frac{\partial\psi}{\partial x}\frac{\partial C}{\partial y}=\frac{1}{Ra\,Le}\nabla^2 C+S_r\nabla^2 T \tag{3}$$

With the boundary conditions:

$$\left.\begin{aligned} &T=C=1,\psi=0 \;\; on\, Y=a\;\sin(N\pi X-\phi);\\ &T=C=\psi=0 \quad on\, Y=1\\ &\frac{\partial T}{\partial X}=\frac{\partial C}{\partial X}=\psi=0 \;\; on\; X=0,1 \end{aligned}\right\} \tag{4}$$

Where the non-dimensional variables and the parameters are defined as follows:

$$\left.\begin{aligned} &X=\frac{x}{L},\; Y=\frac{y}{L},\; T=\frac{t-t_a}{t_w-t_a},\; C=\frac{c\;-\;c_a}{c_w-c_a}, Ra=\frac{Kg\beta\Delta tL}{\nu\alpha},\\ &U=\frac{u}{V_c},\; V=\frac{\mathrm{v}}{V_c} \text{ where } V_c=\frac{g\beta K\Delta t}{\nu},\; \frac{\partial\psi}{\partial Y}=U,\quad \frac{\partial\psi}{\partial X}=-V.\\ &B=\frac{\beta_c\left(c_w-c_a\right)}{\beta_t\left(t_w-t_a\right)}, Le=\frac{\alpha}{D}, D_f=\frac{DK_T\left(c_w-c_a\right)}{C_sC_p\left(t_w-t_a\right)}, S_r=\frac{DK_T\left(t_w-t_a\right)}{C_sC_p\left(c_w-c_a\right)} \end{aligned}\right\} \tag{5}$$

The cumulative global heat flux and the cumulative global mass flux are computed by the formula:

$$QH_X = \int_0^X \left(-\frac{\partial T}{\partial n}\right)\Big|_{Y=a\sin(N\pi x-\phi)} \frac{dS(\xi)}{d\xi} d\xi,\ QM_X = \int_0^X \left(-\frac{\partial C}{\partial n}\right)\Big|_{Y=a\sin(N\pi x-\phi)} \frac{dS(\xi)}{d\xi} d\xi \qquad (6)$$

where '*n*' is the outward normal to the wavy surface and *S*(ξ) is the arc-length along the surface. *X* = 1 i.e. the upper limit gives the global heat flux or the Nusselt number (*Nu*) and global mass flux or the Sherwood Number (*Sh*). The mathematical model is solved by finite element method.

## 3. FINITE ELEMENT FORMULATION

Let $\Omega$ denote the domain of interest and $\Gamma$ be the boundary of the domain. The discretized representation of $\Omega$ is given by $\overline{\Omega} = \bigcup_{e=1}^{NEL} \Omega^e$ where $\Omega^e$ denotes a typical bilinear element of the discretized domain and *NEL* is total number of such elements. The discretized elements are fully disjoint i.e. $\bigcap_e \Omega^e = \{\}$. The discretized representation of the field variables $\psi$, T, C on a typical bilinear element $\Omega^e$ is:

$$\psi = \sum_{i=1}^{4} \psi_i^e N_i^e,\ T = \sum_{i=1}^{4} T_i^e N_i^e,\ C = \sum_{i=1}^{4} C_i^e N_i^e \qquad (7)$$

where $N_i^e$ denotes the standard bi-linear interpolation function on a typical element $\Omega^e$.

Now consider the Galerkin Weighted Residual form of the governing equations (1)-(3) on a $\Omega^e$:

$$\int_{\Omega^e} \left(\frac{\partial^2 \psi}{\partial X^2} + \frac{\partial^2 \psi}{\partial Y^2} - \frac{\partial T}{\partial Y} - B\frac{\partial C}{\partial Y}\right) W_i \, d\Omega^e = 0 \qquad (8)$$

$$\int_{\Omega^e} \left\{\left(\frac{\partial \psi}{\partial Y}\frac{\partial T}{\partial X} - \frac{\partial \psi}{\partial X}\frac{\partial T}{\partial Y}\right) - \frac{1}{Ra}\left(\frac{\partial^2 T}{\partial X^2} + \frac{\partial^2 T}{\partial Y^2}\right) - D_f\left(\frac{\partial^2 C}{\partial X^2} + \frac{\partial^2 C}{\partial Y^2}\right)\right\} W_i \, d\Omega^e = 0 \qquad (9)$$

$$\int_{\Omega^e} \left\{\left(\frac{\partial \psi}{\partial Y}\frac{\partial C}{\partial X} - \frac{\partial \psi}{\partial X}\frac{\partial C}{\partial Y}\right) - \frac{1}{RaLe}\left(\frac{\partial^2 C}{\partial X^2} + \frac{\partial^2 C}{\partial Y^2}\right) - S_r\left(\frac{\partial^2 T}{\partial X^2} + \frac{\partial^2 T}{\partial Y^2}\right)\right\} W_i \, d\Omega^e = 0 \qquad (10)$$

On rewriting the equations (8)-(10) in the weak form and on introducing the element level discretized representation for the field variables i.e. (7) into these modified equations one would arrive at the following element matrix equation:

$$M^e a^e = f^e \tag{11}$$

Where

$$M^e_{ij} = \begin{bmatrix} A_{ij}^{11} & A_{ij}^{12} & A_{ij}^{13} \\ 0 & A_{ijk}^{22} & A_{ij}^{23} \\ 0 & 0 & A_{ijk}^{33} \end{bmatrix} \tag{12}$$

$$a_j^e = \begin{bmatrix} \psi_j^e & T_j^e & C_j^e \end{bmatrix}^T \tag{13}$$

$$f_i^e = \begin{bmatrix} f_i^1 & f_i^2 & f_i^3 \end{bmatrix}^T \tag{14}$$

here,

$$A_{ij}^{11} = \int_{\Omega^e} -\left(\frac{\partial N_i^e}{\partial X}\frac{\partial N_j^e}{\partial X} + \frac{\partial N_i^e}{\partial Y}\frac{\partial N_j^e}{\partial Y}\right) d\Omega^e \tag{15}$$

$$A_{ij}^{12} = \int_{\Omega^e} -\left(N_i^e \frac{\partial N_j^e}{\partial Y}\right) d\Omega^e \tag{16}$$

$$A_{ij}^{13} = \int_{\Omega^e} -\left(BN_i^e \frac{\partial N_j^e}{\partial Y}\right) d\Omega^e \tag{17}$$

$$A_{ijk}^{22} = \int_{\Omega^e} \left(\left\{\sum_{k=1}^{4}\left(\frac{\partial N_k^e}{\partial Y}\frac{\partial N_j^e}{\partial X} - \frac{\partial N_k^e}{\partial X}\frac{\partial N_j^e}{\partial Y}\right)\psi_k^e\right\} N_i^e\right) d\Omega^e + \int_{\Omega^e} \left(\frac{1}{Ra}\left(\frac{\partial N_i^e}{\partial X}\frac{\partial N_j^e}{\partial X} + \frac{\partial N_i^e}{\partial Y}\frac{\partial N_j^e}{\partial Y}\right)\right) d\Omega^e \tag{18}$$

$$A_{ijk}^{23} = \int_{\Omega^e} D_f \left(\frac{\partial N_i^e}{\partial X}\frac{\partial N_j^e}{\partial X} + \frac{\partial N_i^e}{\partial Y}\frac{\partial N_j^e}{\partial Y}\right) d\Omega^e \tag{19}$$

$$A_{ijk}^{32} = \int_{\Omega^e} -S_r \left(\frac{\partial N_i^e}{\partial X}\frac{\partial N_j^e}{\partial X} + \frac{\partial N_i^e}{\partial Y}\frac{\partial N_j^e}{\partial Y}\right) d\Omega^e \tag{20}$$

$$A_{ijk}^{33} = \int_{\Omega^e} \left(\left\{\sum_{k=1}^{4} \left(\frac{\partial N_k^e}{\partial Y}\frac{\partial N_j^e}{\partial X} - \frac{\partial N_k^e}{\partial X}\frac{\partial N_j^e}{\partial Y}\right)\psi_k^e\right\} N_i^e\right) d\Omega^e$$

$$- \int_{\Omega^e} \left(\frac{1}{Ra\,Le}\left(\frac{\partial N_i^e}{\partial X}\frac{\partial N_j^e}{\partial X} + \frac{\partial N_i^e}{\partial Y}\frac{\partial N_j^e}{\partial Y}\right)\right) d\Omega^e \tag{21}$$

In view, of the numerical boundary conditions and their subsequent treatment in the solution process one may take without any loss of generality the r.h.s vector to be a zero i.e. $\left(f_i^1, f_i^2, f_i^3\right) = (0,0,0)$ (22)

The non-linear global system obtained by assembling the local elemental matrix systems (12) is solved iteratively by out of core frontal method for non-linear symmetrical systems to an accuracy of $\varepsilon = 5\times10^{-5}$ on the relative error of nodal field variables from successive iteration i.e. $|\xi_i^{n+1} - \xi_i^n| \le \varepsilon$ where $\xi_i^n = \psi_i^n(or)T_i^n(or)C_i^n$ . Here the superscript n refers to the iteration level and .i refers to the nodal point index.

## 4. RESULTS AND DISCUSSION

The various parameters that govern the double diffusive natural convection under the influence of Soret and Dufour effects in a vertical square porous enclosure, with wavy left wall, are *B* (buoyancy ratio), *Le* (Lewis Number), *Ra* (Rayleigh Number), $D_f$ (Dufour Number), $S_r$ (Soret Number) Number of waves per unit length (*N*), wave amplitude (*a*) and wave phase ($\phi$). Numerical simulations have been made for a wide range of these parameters to analyse the influence of Soret and Dufour effects on

combined heat and mass transfer due to natural convection in a vertical wavy porous enclosure. For now, as per the literature [13-18] we take Ra to be $o(1)$. To begin with a grid selection test has been carried out. Five different grid systems consisting of $21\times21, 31\times31, 41\times41, 51\times51, 61\times61$ grid points have been considered. On these grid systems simulations have been carried out for various combinations of parameters and found that in all the cases the grid system $41\times41$ is adequate. Even as one moves away from the $31\times31$ to higher grid systems in all most all cases only a small change less than1% in the field variable is noticed. As a sample in Table 1 we provide the comparison of Nusselt Number values calculated on different grid systems for a set of parameters. As a matter of fact grid validation tests have been carried out in even under different physical situations too [23-24].

.

| Grid Size | Nusselt Number |
|---|---|
| $21\times21$ | 1.724276 |
| $31\times31$ | 1.790972 |
| $41\times41$ | 1.818385 |
| $51\times51$ | 1.831584 |
| $61\times61$ | 1.832649 |

Table 1: Nusselt Number Values on different grid system for *Ra* = 100, *a* = 0.5, *N* = 1, *Le* = 1, $S_r = D_f = B = 0$.

| Rayliegh Number | Wolker & Homsy [28 ] | Trevisan & Bejan [27 ] | Beckermann Et al [25 ] | Shiralkar Et al [ 26] | Present study |
|---|---|---|---|---|---|
| 50 | 1.98 | 2.02 | 1.981 | - | 1.966 |
| 100 | 3.09 | 3.27 | 3.113 | 3.118 | 3.028 |
| 200 | 4.89 | 5.61 | 5.038 | 4.976 | 5.448 |
| 500 | 8.66 | - | 9.308 | 8.944 | 8.348 |

Table 2: Comparison of Nusselt Number values with those from literature for *Ra* = 100, *a* = 0.0, *N* = 1, *Le* = 1, $S_r = D_f = B = 0$.

Further we also validate the code on the chosen $41 \times 41$ grid system with the results as available from the literature. Table 2 presents one such comparison of Nusselt Number values.

To begin with, we look at the influence of Soret effect fixing $D_f$ = 0.5, *Le, N, B* = 1, *a* = 0.1. In figs (2-3) cumulative heat flux ($QH_X$) and mass flux ($QM_X$) along the wavy vertical wall has been plotted for $0.1 \le S_r \le 4.0$. While $QH_X$ increases with increasing soret effect $QM_X$ is seen to decrease. $QH_X$ plots project the presence thermal boundary layer near the hot wavy wall. These thermal boundary layers get increasingly sharp with increasing values of $S_r$. $QM_X$ plots also project the presence of concentration boundary layers but unlike to the thermal gradients, here the mass gradients are seen to smaller with increasing $S_r$ thereby leading to the loss in the sharpness in concentration boundary layers. Also the plots project that while the local heat fluxes tend to get marginal, especially after nearly half the distance from the lead edge of the wavy wall, the concentration fluxes tend remain relatively significant even far away from the leading edge of the wavy wall. In fig (4) variation in *Nu* and *Sh* with increasing values of $S_r$ is presented. Clearly while *Nu* increases with increasing values of $S_r$, *Sh* are seen to decrease. In order to get a deeper insight it is better to trace the temperature and concentration variable fields. In figs (5-7) we present the streamlines, isotherms and iso-concentration contours for the current set of parameter values. From the streamlines we notice that with increasing $S_r$ the uni-cellular flow circulation pattern changes to a multi-cellular pattern. The eye of the primary circulation also drifts from the lower left corner towards the top wall with a marked change in the flow orientation. From the isotherms and iso-concentration contours one can find that with increasing values of $S_r$, while the iso-concentration contours lead to the formation of two localized patterns, one along the wavy wall and the other near the top right corner of the enclosure, the isotherms spread shifts from the bottom-top orientation to a completely diagonal path starting from

the left bottom corner of the wavy isothermal wall. The isotherms clearly depict the presence of increasingly sharper thermal boundary layers. The variation in the isotherm line alignment depicts the situation of increased heat flux into the domain. The Iso-concentration contours depict the situation of reduced concentration flux into the domain and clearly justify the observed reduction in the *Sh* with increasing values of $S_r$. Increase in Soret effect favors a quick spread and thus stabilization in masses. In effect with the additional diffusion of matter, due to temperature gradients in the domain, there is an increased heat flux along the hot wavy wall. Contour plots clearly depict the sensitivity of the field variables are significantly influenced by the Soret effect.

Next, we look at the influence of Dufour Number ($D_f$) fixing $S_r$ = 0.5, *Le, N, B* = 1, *a* = 0.1. In the fig (8) cumulative heat fluxes ($QH_X$) along the wavy vertical wall has been plotted for $0.1 \le D_r \le 2.0$. $QH_X$ is seen to increase with increasing $D_f$. The plots in the fig (9) illustrate the variation of *Nu* and *Sh* with $D_f$ is presented. While there is a slight increase in *Nu* values, the variation in the *Sh* value is marginal. Streamlines, isotherms and iso-concentration contours for $D_f$ = 0.1, 8.0 are presented in fig (10). The variation in isotherm alignment clearly depict that the temperature field is sensitive to $D_f$ magnitude. The diagonal shift observed in the isotherm pattern with increasing values of $D_f$ supports the observed increase in the heat fluxes along the wavy wall. However, other field variables remain nearly unaffected. Hence the additional diffusion of heat brought in by the concentration gradients primarily affects the temperature field leaving other fields nearly unaltered.

In figs (11-12) variation in the cumulative heat and mass fluxes along the wavy wall with increasing values of *N* are presented for $D_f$, $S_r$ = 0.5, *Le, N, B* = 1, *a* = 0.1 and $1 \le N \le 6$. Both the fluxes decrease with increasing values of *N*. The nearly smooth stair case nature in the heat/mass flux plots is due to periodic boost to the thermal/mass related buoyancy forces along the wavy wall. The positive slope of the tangent to the wavy surface indicates the presence of favorable additional buoyancy forces, as they are in the upward

direction like those of gravitational buoyancy forces. While one moves from crest to trough the slope is positive and hence there is a raise in the heat/mass flux corresponding to this region. To further analyze the net fall in the heat/mass fluxes with increasing *N* the corresponding flow, temperature and concentration fields are tracked through streamlines, isotherms and iso-concentration contours in the plots of figs (13-15). Streamline plots in fig (13) depict the manifestation of complex multi-cellular circulation pattern, which can go onto hinder; the heat/mass transfer into the core of the domain. Isotherm/Iso-concentration patterns depict a loss in heat/mass flux favoring thermal/concentration boundary layer and a localization of heat/mass with increasing values of *N*.

Finally, the influence of *Le* and *B* on heat/mass fluxes in the presence of both Soret and Dufour effects for $D_f, S_r = 0.5$, $N = 1$, $a = 0.1, 0.1 \le Le \le 4$, $-2 \le B \le 2$ are analyzed. In fig (16) the variation of *Nu* and *Sh* with *Le* and *B* are presented. While *Nu* is seen to increase with increasing either *Le* or *B*, *Sh* is seen to decrease. This is exactly contrary to what is observed in the absence of Soret and Dufour effects. So to further analyze the influence of *Le* on the distribution of the field variables streamlines, isotherms and iso-concentration plots traced and presented in figs (17-19). While the isotherms get shifted from vertical to diagonal orientation, iso-concentration contours get into two localized patterns. Streamlines depict the development of complex multiple circulation zones with increasing Le. All the field variables are sensitive the magnitude of the variation in the ratio of thermal to mass diffusivities. Any increase in thermal diffusivity co-efficient and any decrease in mass diffusivity co-efficient are seen to enhance/reduce heat/mass fluxes into the domain. On increasing *B,* in the presence of Soret and Dufour effects, while *Nu* is marginally increasing *Sh* is seen to marginally decreasing. With varying *B* as opposing thermal and species buoyancy forces begin to aid each other the flow pattern is seen to get complex with horizontal circulation patterns.

# Conclusions

A numerical study based on finite element computation has been carried out to investigate the influence of Soret and Dufour effects on double diffusive natural convection induced by an isothermal wavy vertical wall in a fluid saturated isotropic corrugated porous enclosure. In the presence of Soret and Dufour effects while Nusselt Number increases with increasing values of $S_r$ , $D_f$ , *Le* and *B* Sherwood Number is found to be decreasing. However, in the presence of Soret and Dufour effects an increase in *N* and thereby the surface roughness, weakens both the heat and mass fluxes into the domain. Interesting features like a diagonal shift in the isotherm patterns, the development of multiple localized iso-concentration patterns and the manifestation of multiple complex circulation patterns in the flow domain are observed. Overall at small values of Ra, the influence of Soret effect on the double-diffusive process is more prominent than that of Dufour effect.

# References


1. A. Bejan & K.R.Khair, IJHMT, 28(5), 909, 1985.
2. A. Nakayama, M. A. Hossain, IJHMT, 38 (4), 761, 1995.
3. D. Angirasa, G.P.Peterson, I.Pop, IJHMT, 40(12), 2755, 1997; NHT: Part A, 34, 1189, 1997.
4. C. Y. Cheng, Int. Comm. HMT 27(8), 1143, 2000.
5. B.V.Rathish Kumar, P. Singh, V. J. Bansod, NHT: Part A, 41, 421, 2002.
6. B.V.Rathish Kumar, P. Singh, V. J. Bansod , JPM 5(1), 57, 2002.
7. E. R.G. Eckert and R. M. Drake, 1972, McGraw Hill, NY.
8. G. Zimmerman and U. Muller, 1992, IJHMT 35, 2245-2256.
9. D.T.Hurle and E. Jakerman, 1989, JFM. 447, 667-687.
10. T. L. Bergman and R. Srinivasan, 1989, IJHMT, 32, 679-687.
11. J. A. Weaver and R. Viskanta, 1991, IJHMT, 34, 3121-3133.
12. L. B. Benano-Melly, J.P. Caltagirone, B. Faissat, F. Montel, and P. Costesque, 2001, IJHMT, 44, 1285.

13. M. Anghel, H.S. Thakar, and I. Pop, 2000, Studia. Universitatis Babes-Bolyai, Mathematica, Vol. XLV, P.11.
14. A. Postelnicu, 2004, IJHMT, 47, 1467-1472.
15. O. Sovran, M.C. Charrier-Mojtabi, A. Mojtabi, 2001, CR Acad, Sci. Paris, 239, p. 287.
16. M.K.Partha, Ph.D.Thesis, IIT-Kgp, India, 2006.
17. D.S. Riley, IJHMT, 31, 1988, 2365-2380.
18. D.A.S. Rees and I. Pop, Fluid Dynamics Research, 14, 1994, 151-166.
19. D. A. S. Rees and I. Pop, ASME J. of Ht. Trans., Vol. 116, PP. 505-508, 1994.
20. B.V. Rathish Kumar, P. Singh and P.V.S.N. Murthy, ASME IJHMT. 199, 1997, 848-851.
21. B.V. Rathish Kumar, P.V.S.N. Murthy and P.Singh, IJNMF, 28, 1998,633-661
22. P. V. S. N. Murthy, B. V. Rathish Kumar and P. Singh, Num. Heat. Transfer, Part A, 31, 207-221, 1997.
23. B. V. Rathish Kumar and Shalini, Applied Mathematics & Computation, Vol. 17(1), pages 180-222, Dec 2005.
24. B. V. Rathish Kumar and Shalini, Journal of Porous Media, vol. 7, issue 4, pp. 13-30, 2004.
25. C. Beckermann, R. Viskanta, and S. Ramadhyani., *Numerical Heat Transfer - A*, 10:557–570, 1986.
26. G. S. Shiralkar, M. Haajizadeh, and C. L. Tien,. *Numerical Heat Transfer - A*, 6:223–234, 1983
27. O. V. Trevisan and A. Bejan., *Int. J. Heat Mass Transfer*, 28:1597–1611, 1985
28. K. L. Walker and G. M. Homsy. *J. Fluid Mech.*,87: 449–474, 1978

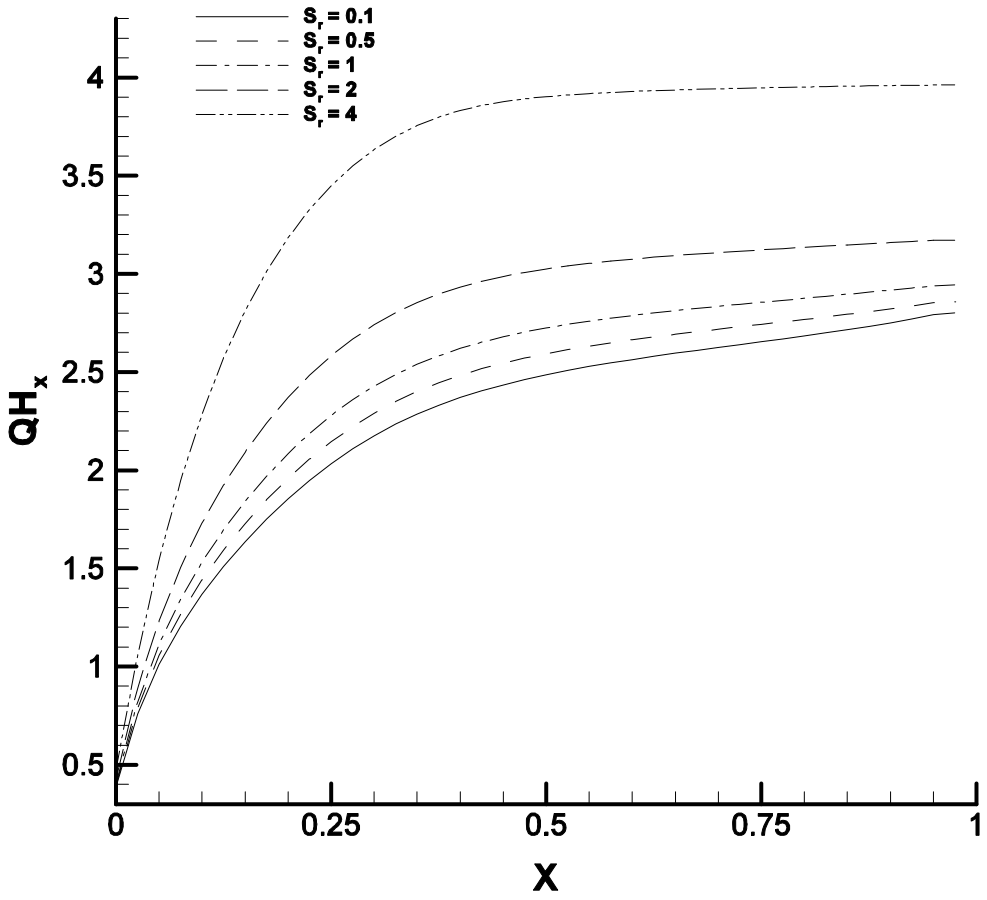



Fig 2: Cumulative heat flux ($QH_X$) along the wavy wall for different values of $S_r$

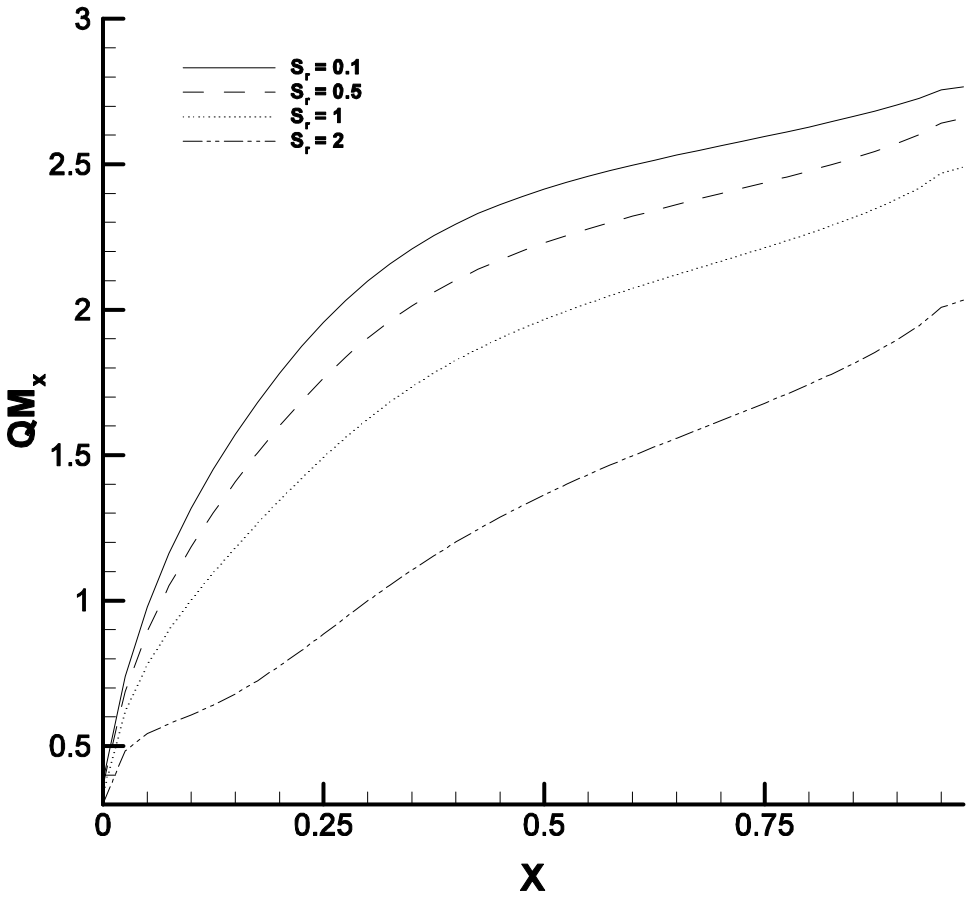



Fig 3: Cumulative mass flux ($QM_X$) along the wavy wall for different values of $S_r$.

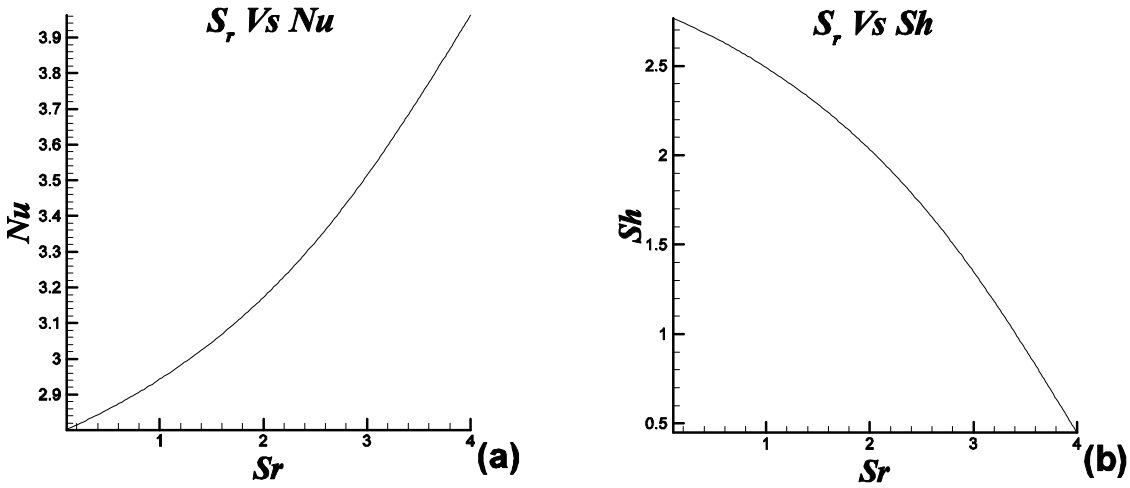



Fig 4: Influence of Soret effect on Global heat flux (*Nu*) and Global Mass flux (*Sh*).

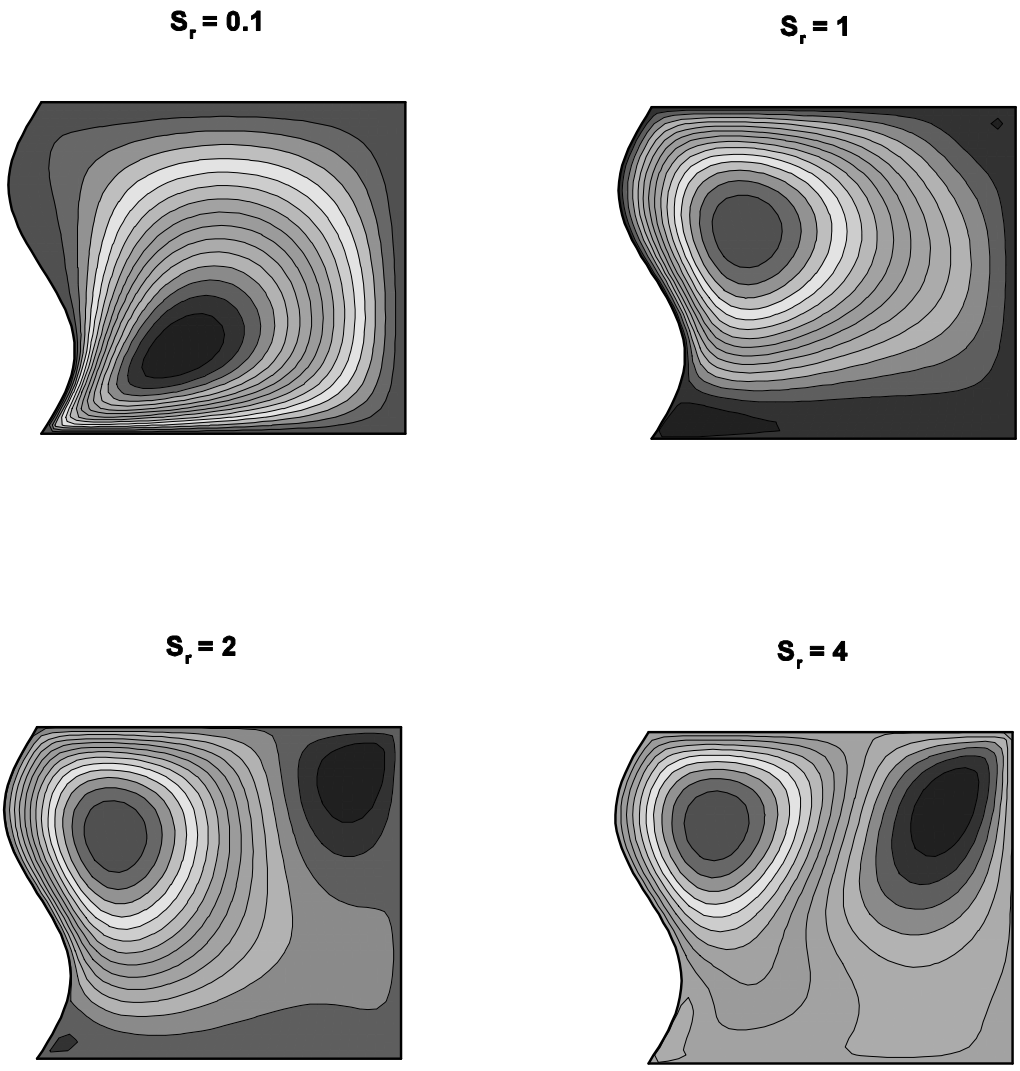



Fig 5: Influence of Soret Effect on flow field traced as streamlines.

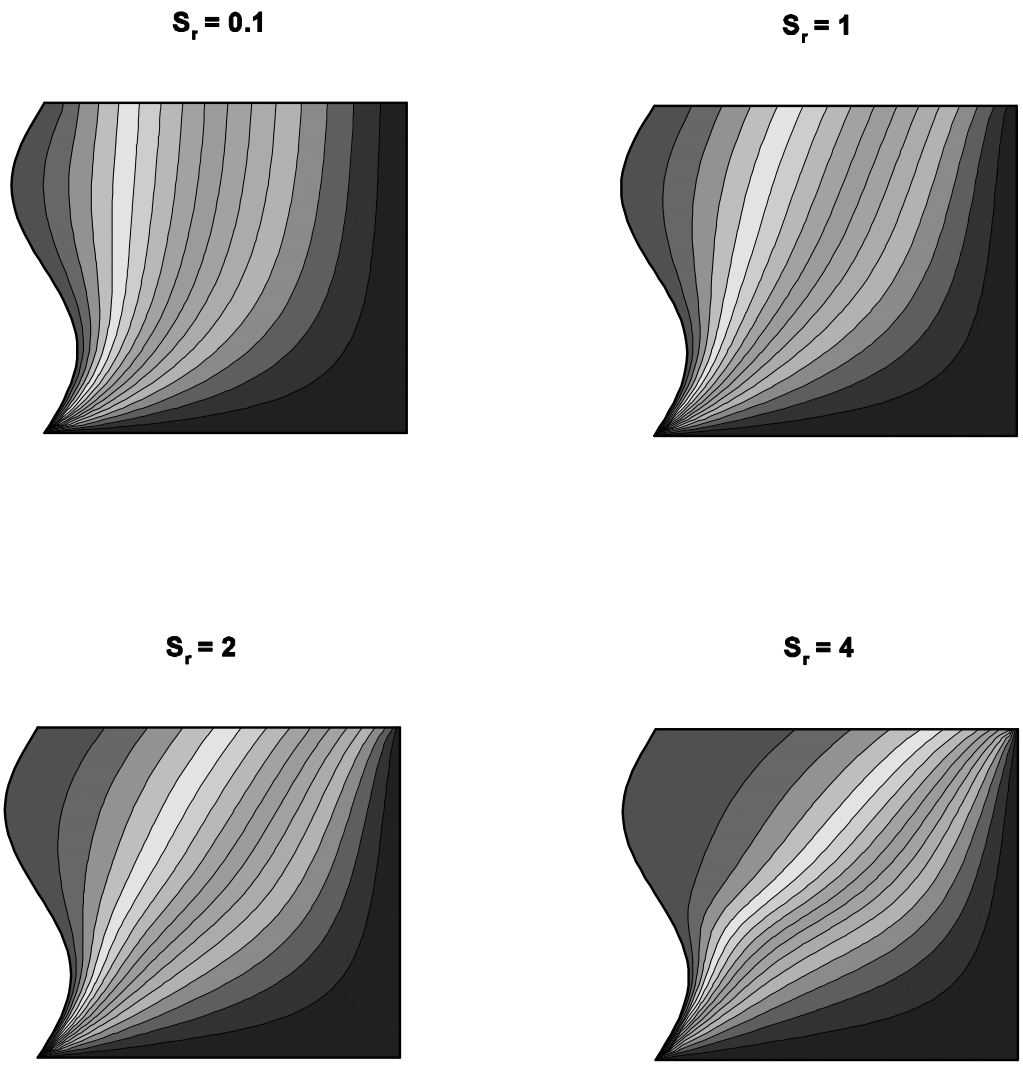



Fig 6: Influence of Soret Effect on Temperature field traced as Isotherms

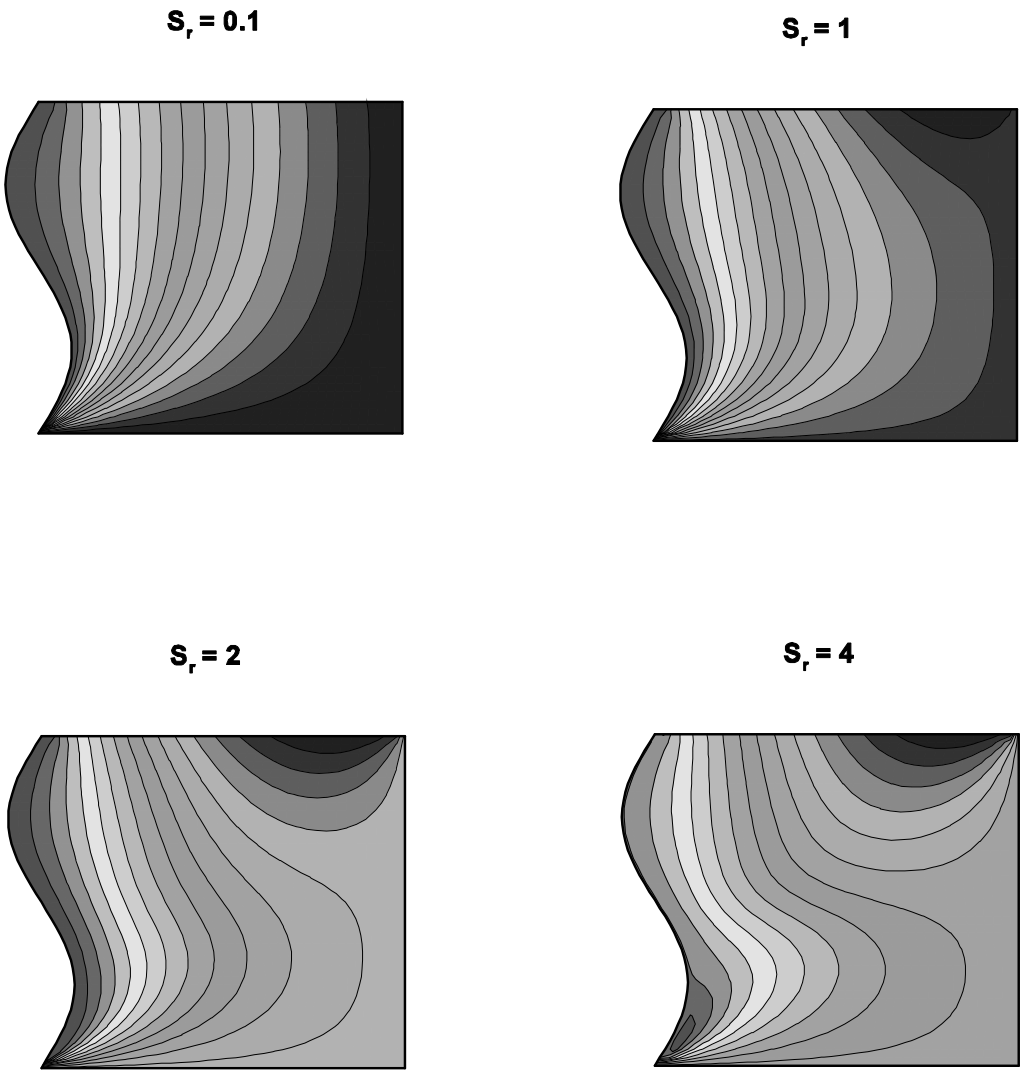



Fig 7: Influence of Soret Effect on Concentration field traced as Iso-Concentration contours.

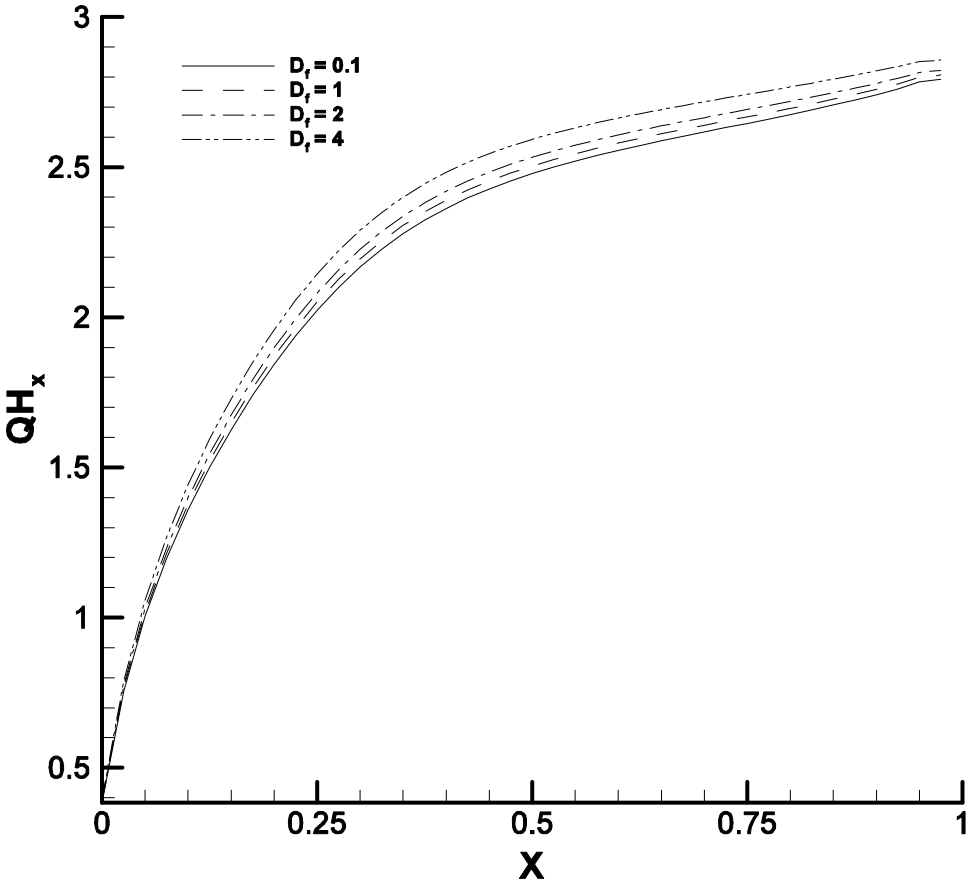



Fig 8: Cumulative heat flux along the wavy wall for different values of $D_f$ .

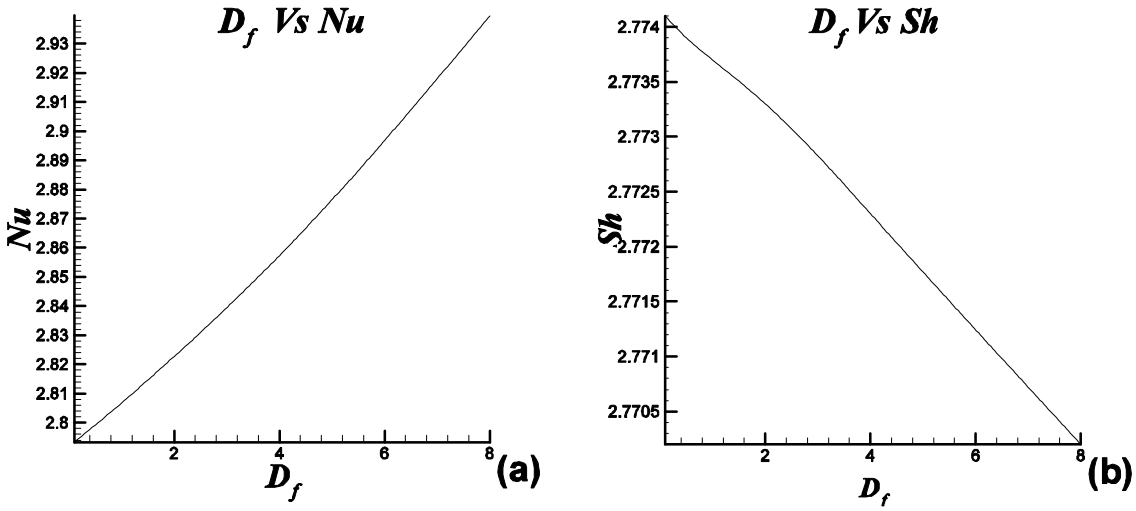



Fig 9: Influence of Dufour Effect on Global Heat Flux (Nu) and Global Mass Flux (*Sh*).

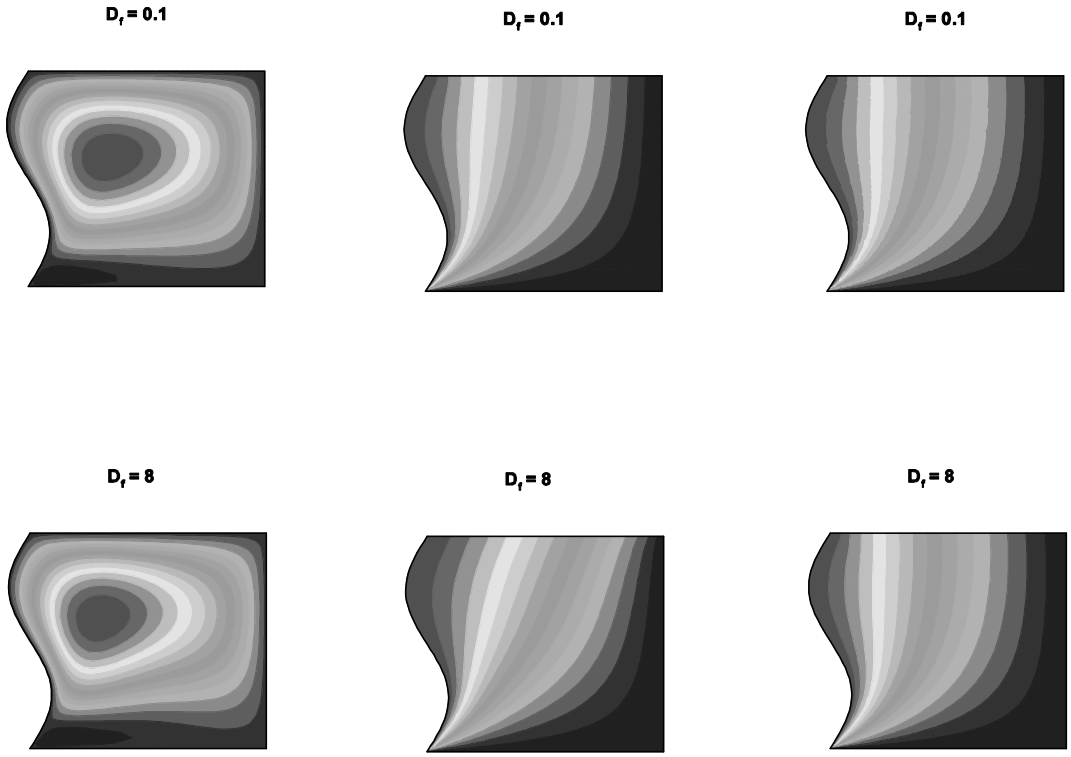



Fig 10: Influence of Dufour effect on flow, temperature and concentration fields traced as streamlines, isotherms and iso-concentration contours respectively.

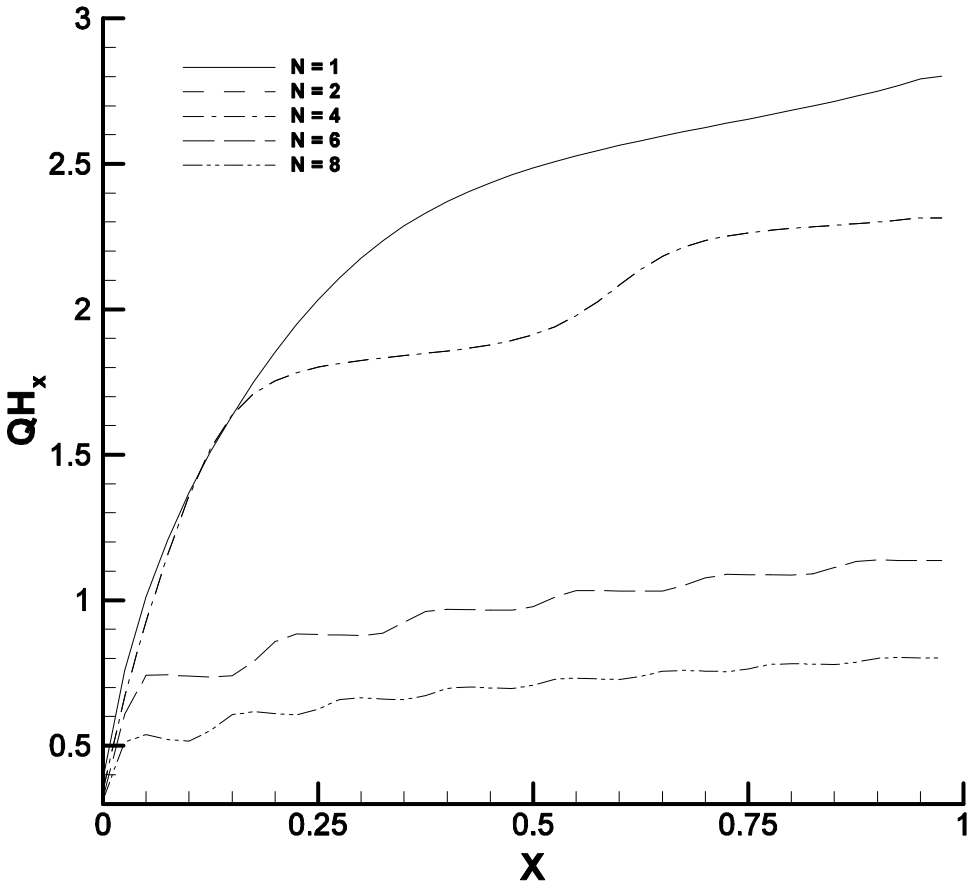



Fig 11: Cumulative Global Heat Flux ( $QH_X$ ) along the wavy wall with increasing level of corrugation along the wavy wall.

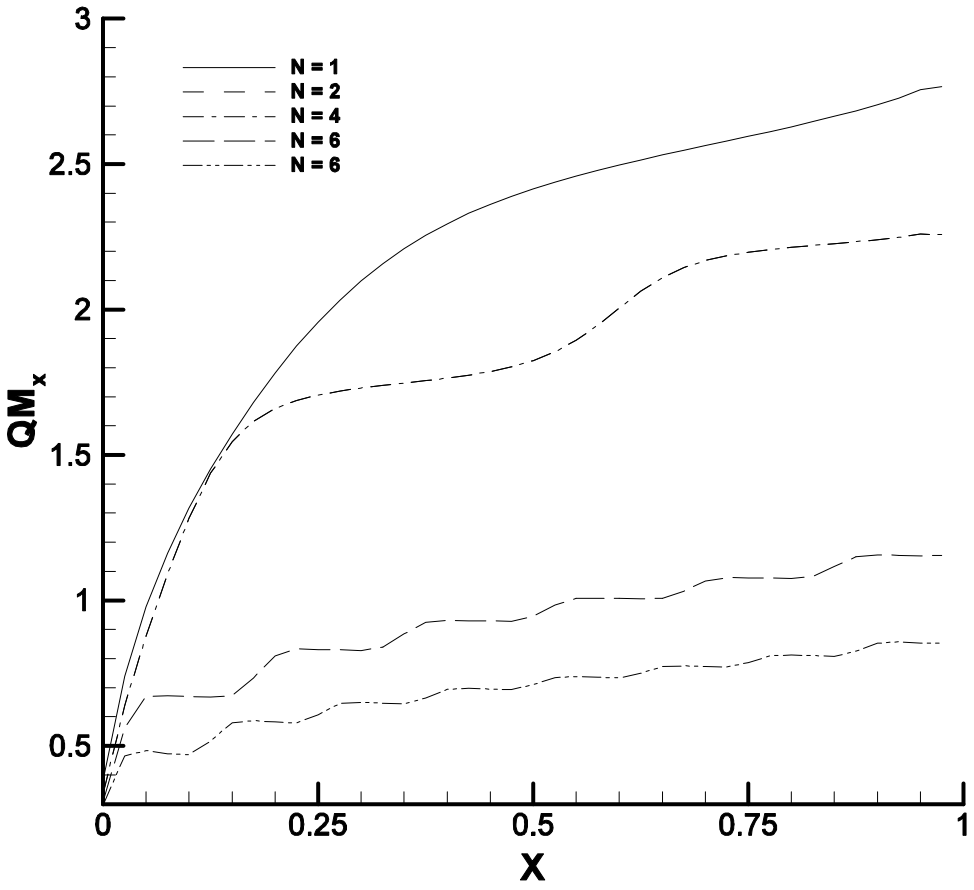



Fig 12: Cumulative Mass Flux ( $QM_X$ ) along the wavy wall with increasing levels of corrugation on the wavy wall.

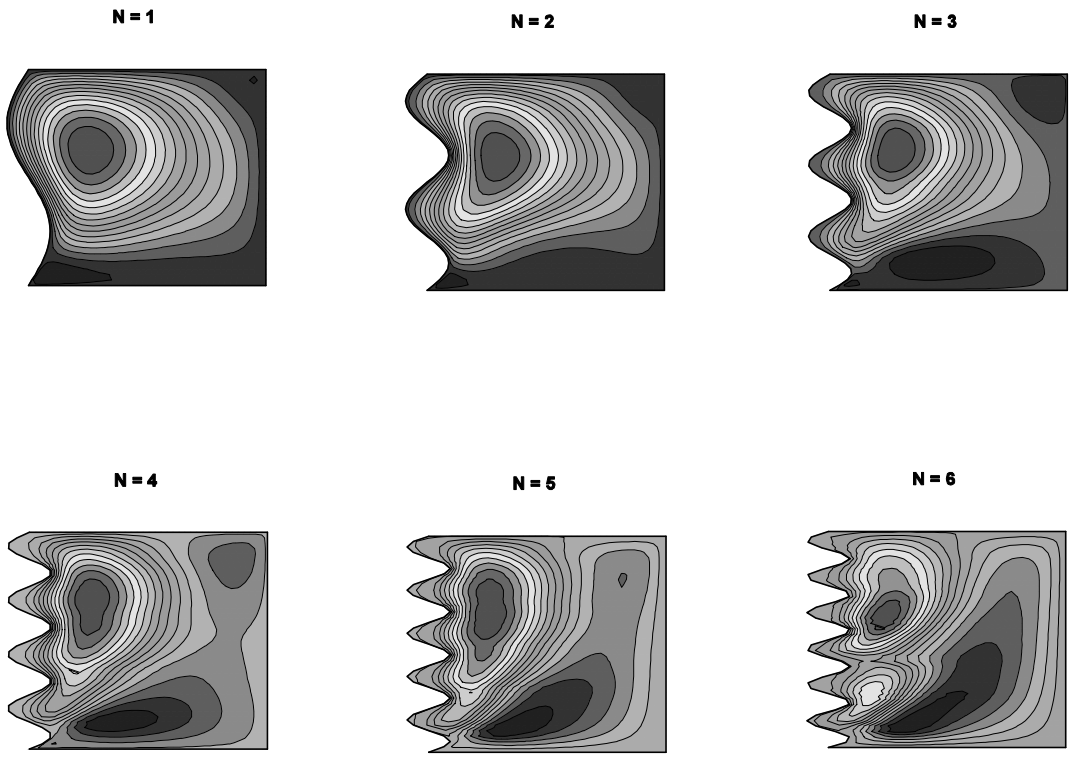



Fig 13: Influence of increasing levels of corrugation on the flow domain traced in the form of streamlines

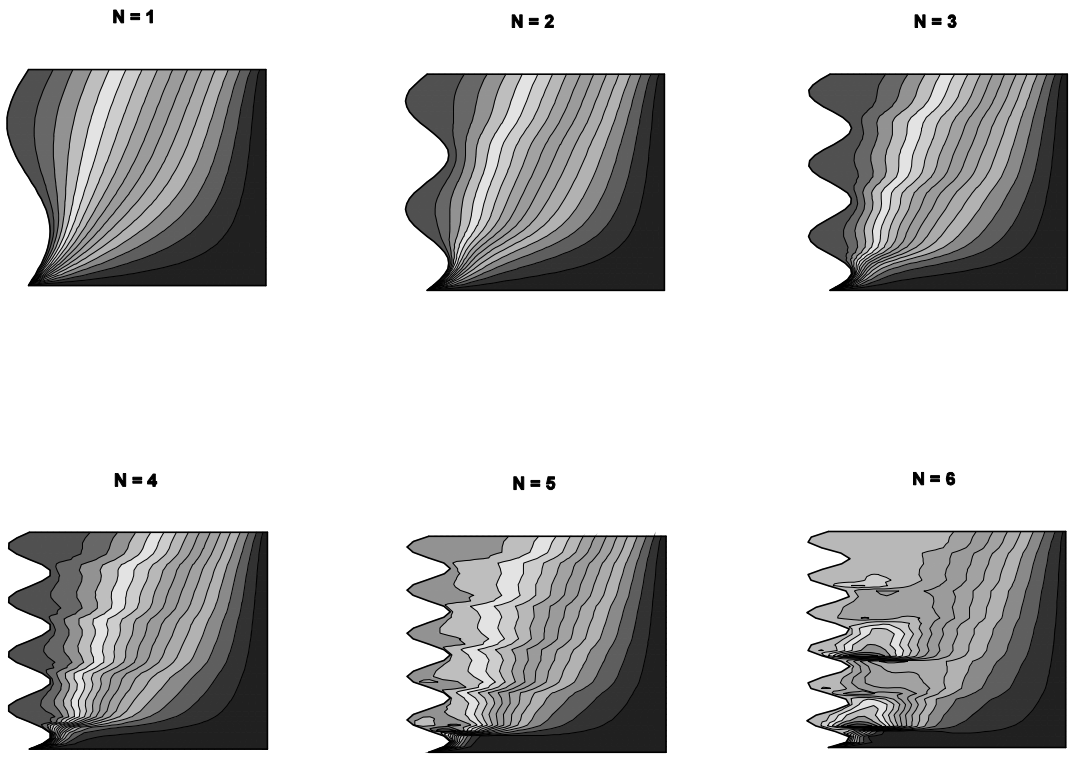



Fig 14: Influence of increasing levels of corrugation on the wavy wall on the temperature field traced as isotherms.

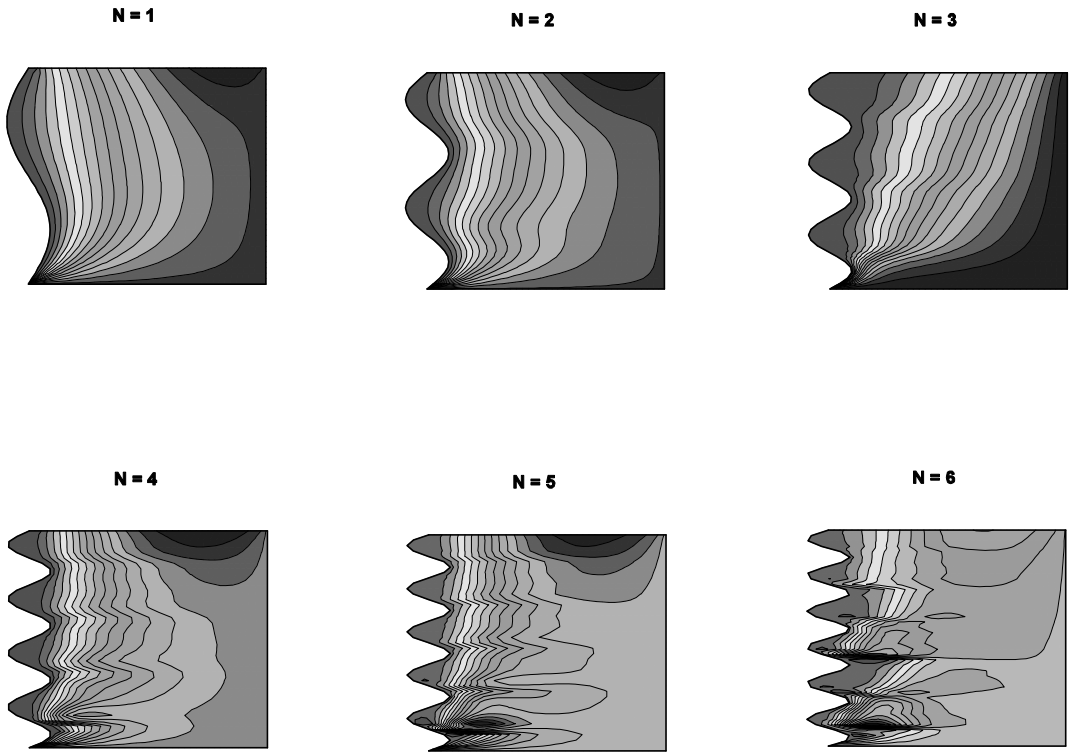



Fig 15: Influence of increasing levels of corrugation on the wavy wall on the concentration field traced in the form of iso-concentration contours

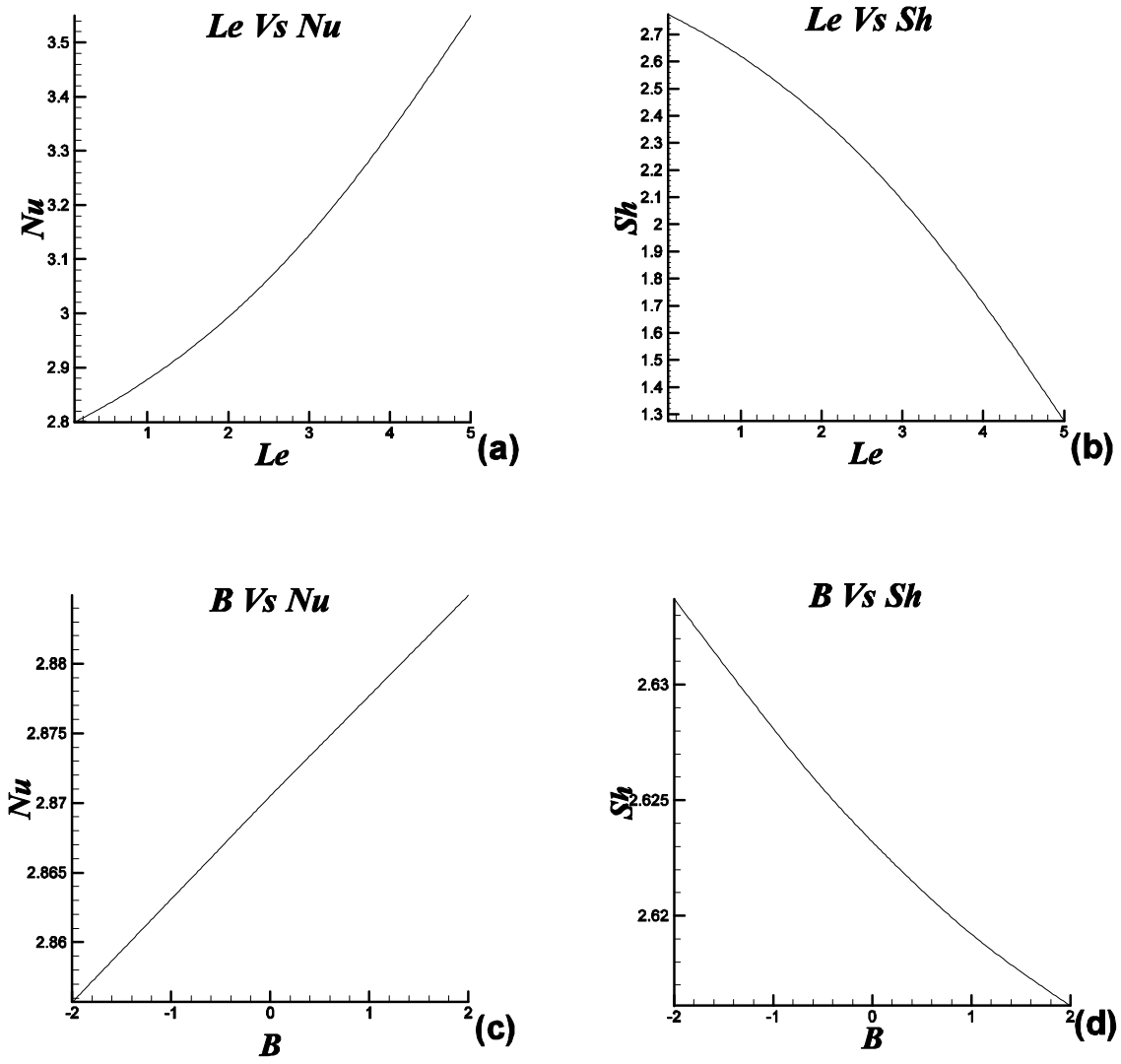



Fig 16: Influence of *Le* and *B* on Global Heat Flux (*Nu*) and Global Mass Flux (*Sh*).

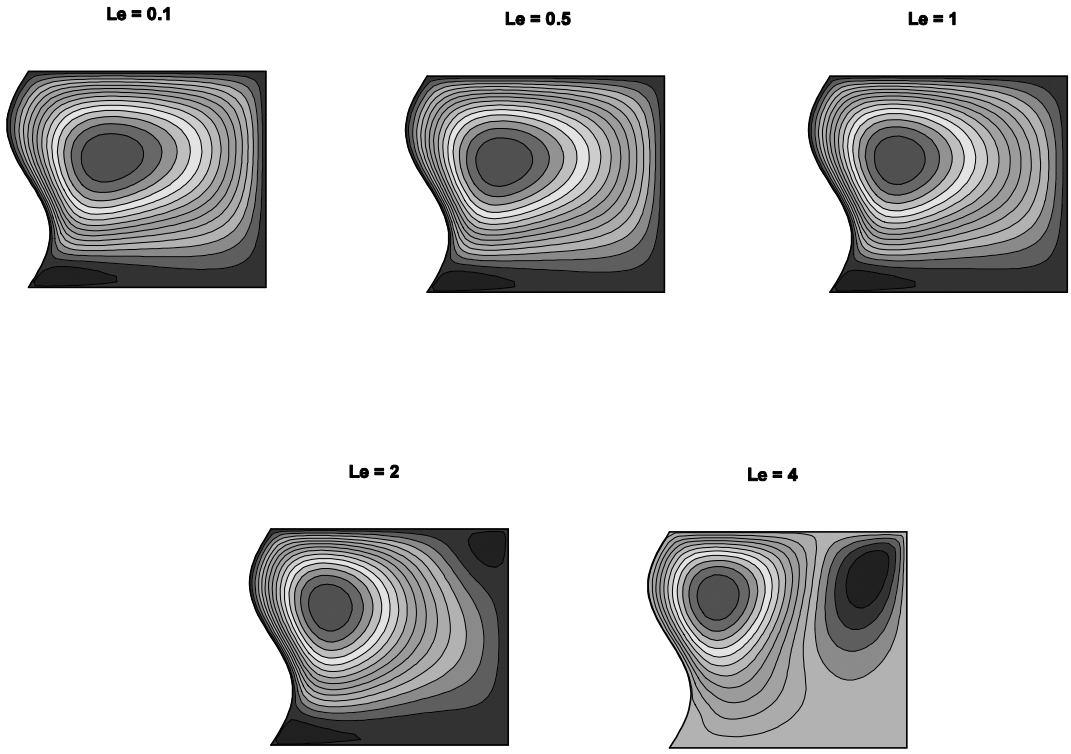



Fig 17: Influence of *Le* on flow field traced in the form of streamlines.

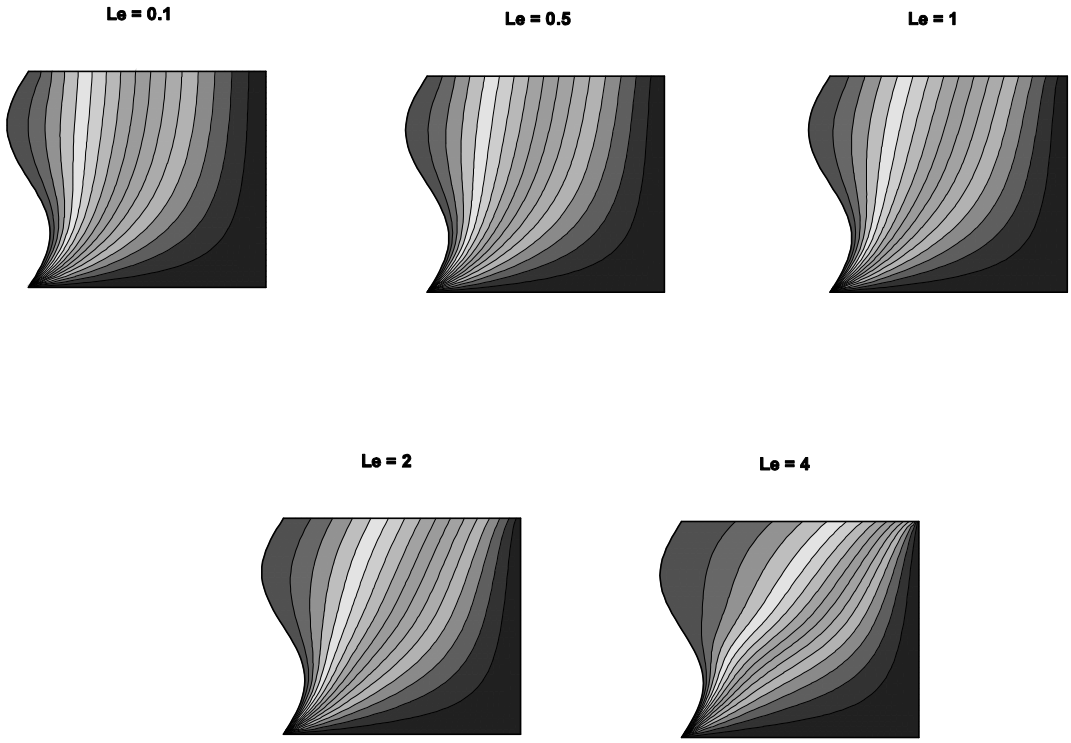



Fig 18: Influence of *Le* on temperature field traced in the form of isotherms.

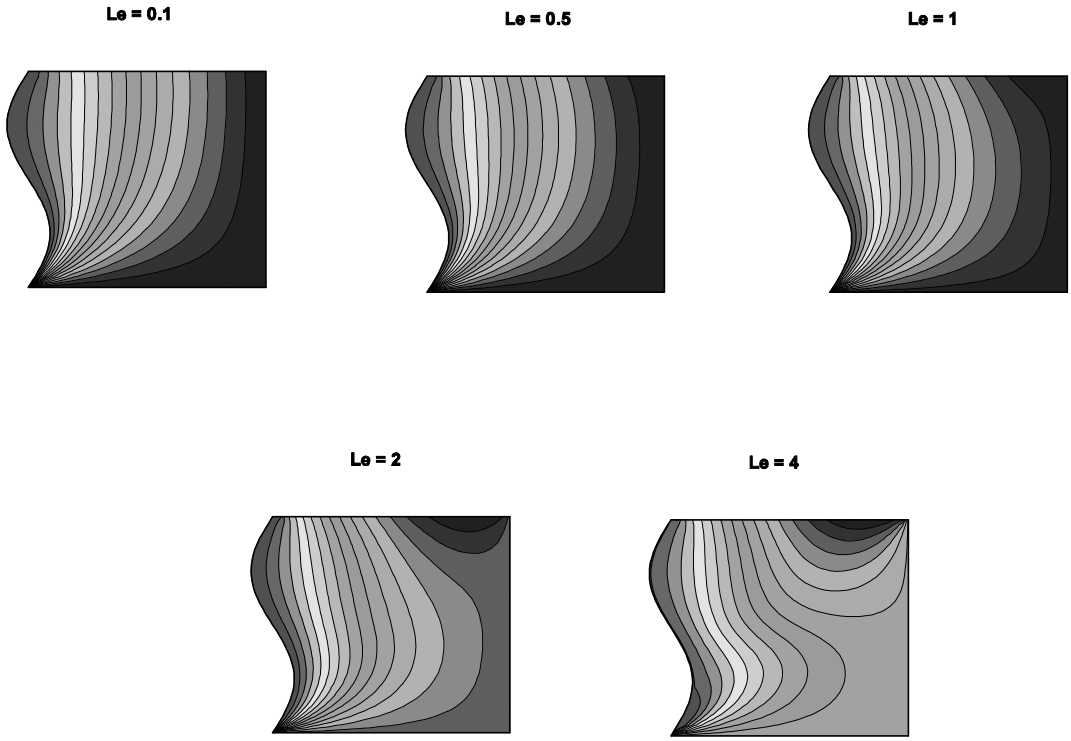



Fig 19: Influence of *Le* on concentration field traced in the form of iso-concentration contours.

This document was created with Win2PDF available at http://www.win2pdf.com.
The unregistered version of Win2PDF is for evaluation or non-commercial use only.
This page will not be added after purchasing Win2PDF.